CORA Cork Open Research Archive
Cartlann Taighde Oscailte Chorcaí

Title	A portable multiplexed electrochemical biosensor for lactate and pH monitoring in calf saliva
Authors	Adib, Md Ridwan;Higes-Marquez, Javier;Barrett, Colm;O'Sullivan, Shane;McFadden, Marie;Kennedy, Emer;O'Riordan, Alan
Publication date	2026-11-01
Original Citation	Adib, M R, Higes-Marquez, J, Barrett, C, O'Sullivan, S, McFadden, M, Kennedy, E & O'Riordan, A 2026, 'A portable multiplexed electrochemical biosensor for lactate and pH monitoring in calf saliva', Biosensors and Bioelectronics, vol. 311, 118965, pp. 1-11. https://doi.org/10.1016/j.bios.2026.118965
Type of publication	Article (peer-reviewed)
Link to publisher's version	https://www.scopus.com/pages/publications/105042793663 - 10.1016/j.bios.2026.118965
Rights	© 2026, authors. Published by Elsevier B.V. This is an open access article under the CC BY license (http://creativecommons.org/licenses/by/4.0/) - https://creativecommons.org/licenses/by/4.0/
Download date	2026-11-14 00:06:43
Item downloaded from	https://hdl.handle.net/10468/19616



UCC
University College Cork, Ireland
Coláiste na hOllscoile Corcaigh

Biosensors and Bioelectronics 311 (2026) 118965

Contents lists available at ScienceDirect

Biosensors and Bioelectronics

journal homepage: www.elsevier.com/locate/bios

A portable multiplexed electrochemical biosensor for lactate and pH monitoring in calf saliva

Md Ridwan Adib [a,*], Javier Higes-Marquez [a], Colm Barrett [a], Shane O'Sullivan [a], Marie McFadden [b], Emer Kennedy [b], Alan O'Riordan [a,**]

[a] Precision Electrochemical Nanosensor Group, Tyndall National Institute, University College Cork, Dyke Parade, Cork, Ireland
[b] Teagasc, Animal & Grassland Research and Innovation Centre, Moorepark, Fermoy, Cork, Ireland

ARTICLE INFO

Keywords:
Electrochemical lactate and pH sensor
pH control
Dual sensing
Saliva
Non-invasive technology
Sensor electronics interface

ABSTRACT

Non-invasive biomarker assessment in saliva offers a promising route for early detection of bovine respiratory disease and scour in calves. However, accurate electrochemical sensing in this complex matrix remains challenging due to variable pH, viscosity, and interfering species. Here, we report an integrated dual-function interdigitated microelectrode (IDE) platform capable of simultaneous detection of lactate and pH, operating under an in-situ electrochemical pH control strategy to regulate the local sensing microenvironment and improve operational stability. Microband Au IDEs were fabricated using multilayer photolithography and metal deposition, followed by sequential surface modification with platinum black, o-phenylenediamine/β-cyclodextrin and lactate oxidase to enable selective and sensitive lactate detection. Finite element simulations confirmed rapid local acidification and oxygen generation at the protonator electrodes, enabling precise pH tuning at the sensing interface. The pH sensor exhibited a linear super Nernstian response from pH 3-9 in buffer (−66.0 mV.pH^{-1}, $R^2 = 0.999$), while the lactate biosensor demonstrated a linear range of 0.02-7 mM in artificial saliva, achieving a limit of detection of 0.6 μM with pH control. A portable, battery-powered electronics interface with wireless data transmission was developed and benchmarked against laboratory instrumentation, achieving comparable sensitivities for lactate (−0.47 nA mM^{-1}) and pH (−117 mV.pH^{-1}) in artificial saliva. In calf saliva, the platform accurately distinguished healthy vs. sick animals, consistent with clinical health scoring. This multiplexed, pH-regulated sensing system offers a robust pathway toward field-deployable, non-invasive diagnostic tools for rapid monitoring of animal health and welfare.

1. Introduction

Early and accurate diagnosis of disease in livestock is essential for improving animal welfare, ensuring sustainable food production, and minimizing economic losses within the agricultural sector (Blakebrough-Hall et al., 2020; Bonilla-Cedrez et al., 2023; Kappes et al., 2023; Lorenz et al., 2011; Singh et al., 2024). In young calves, illnesses such as bovine respiratory disease (BRD) and neonatal diarrhoea (scour) account for a substantial proportion of morbidity and mortality during the pre-weaning period ("All-Island Animal Disease Surveillance Report," 2022; "Department of Agriculture, Food, and the Marine Report," 2022; Attree et al., 2024; Roblin et al., 2023). These conditions often develop rapidly and can progress before overt clinical signs appear, making timely detection crucial for effective intervention. Conventional diagnostic strategies frequently rely on invasive sampling (Doyle et al., 2017; Pardon and Buczinski, 2020), intermittent clinical observations (Berman, 2024; Otten et al., 2023), or laboratory-based biochemical analysis (Li et al., 2022; Shehta et al., 2022), all of which can delay decision-making and may not capture the dynamic physiological changes occurring during disease onset. Consequently, there is a growing need for non-invasive, real-time biosensing platforms capable of continuous or repeated monitoring of health-relevant biomarkers directly at the point of care.

Saliva has emerged as an attractive medium for non-invasive physiological assessment in both humans and animals. It contains a diverse panel of biomarkers including enzymes, metabolites, electrolytes, hormones, inflammatory mediators, DNA, RNA, and microorganisms that together reflect systemic health status (d'Amone et al., 2021;

* Corresponding author.
** Corresponding author.
E-mail addresses: ridwan.adib@tyndall.ie (M.R. Adib), alan.oriordan@tyndall.ie (A. O'Riordan).

https://doi.org/10.1016/j.bios.2026.118965
Received 11 March 2026; Received in revised form 23 June 2026; Accepted 25 June 2026
Available online 27 June 2026
0956-5663/© 2026 The Authors. Published by Elsevier B.V. This is an open access article under the CC BY license (http://creativecommons.org/licenses/by/4.0/).

Dongiovanni et al., 2023; Song et al., 2023; Zhou and Liu, 2023). Among these, lactate has become a key biomarker for assessing metabolic stress, tissue oxygenation, immune response, and the onset of infectious diseases (Ghimenti et al., 2020). Elevated salivary lactate concentrations have been associated with systemic inflammation, respiratory distress, dehydration, and impaired energy metabolism (Contreras-Aguilar et al., 2019). Salivary pH is also highly informative: fluctuations in pH reflect alterations in microbial load, metabolic acidosis, digestive disturbances, and hydration status, all of which accompany BRD and scour (Castillo-Lopez et al., 2021; Riley et al., 2024). Combined measurement of lactate and pH therefore provides an enhanced diagnostic picture, offering a more robust assessment of calf health than either parameter alone. Despite these opportunities, the direct electrochemical measurement of lactate and pH in saliva is technically challenging. Saliva is a complex, heterogeneous fluid whose viscosity, protein content, pH, and ionic strength can negatively influence sensor stability and accuracy. The intrinsic viscosity of saliva slows diffusion of electroactive species toward the electrode surface, suppressing faradaic currents and degrading analytical sensitivity (Chang et al., 2023). pH variability directly alters enzyme activity, particularly that of lactate oxidase (LOx), which exhibits optimal catalytic performance near neutral pH (Ike et al., 2025). Additionally, common salivary interferents such as ascorbic acid (AA), uric acid (UA), D-fructose (D-Fruc), D-glucose (D-Glu), and acetaminophen (Ace) can be oxidized at similar potentials to hydrogen peroxide (H_2O_2), generating false-positive or distorted signals in first-generation enzymatic sensors. (Arakawa et al., 2016; Barrett et al., 2015; Pietraforte et al., 2006; Stoytcheva et al., 2025). These challenges severely restrict the deployment of conventional amperometric lactate sensors in saliva without additional processing steps or chemical pretreatment.

Beyond matrix-related complexity, the physicochemical characteristics of both salivary lactate and pH create additional sensing challenges. Salivary lactate concentrations in calves generally fall within 0.15-0.78 mmol.L^{-1}, markedly lower and more variable than circulating blood lactate levels, which typically range from 0.5 to 2.0 mmol.L^{-1} (Contreras-Aguilar et al., 2021; Omole et al., 2001). Current clinical approaches for lactate measurement rely on invasive procedures: blood is typically drawn and analyzed using blood analyzers, or via benchtop commercial systems capable of measuring lactate in blood, serum, or plasma (Joseph et al., 2025; Mentzoni et al., 2024). These methods are unsuitable for repeated or on-farm monitoring due to the need for blood extraction, sample handling, trained personnel, and centralized analysis. Non-enzymatic lactate sensors have been explored, but they generally suffer from poor selectivity, narrow linear ranges, and pronounced surface fouling in mucin- and protein-rich saliva (Dokur et al., 2025; Sapurta and Karim, 2025). LOx-based enzymatic sensors, while more selective, rely heavily on the local biochemical environment. Oxygen is required to regenerate the oxidized enzyme during catalysis, and limited oxygen availability can constrain the maximum enzymatic turnover rate in viscous or poorly aerated media such as saliva, making sensor responses more variable (Malon et al., 2014; Yang and Yan, 2025). Furthermore, deviations in local pH at the electrode interface rather than bulk salivary pH alone can alter LOx catalytic efficiency and shift electrode kinetics, leading to variability in sensor response and false positives/negatives. Collectively, these factors underscore the need for sensor architectures that can stabilize enzymatic function, regulate local pH, and minimize interference within complex salivary matrices. Alternative strategies for lactate and pH analysis have included colorimetric assays, wearable optical platforms, microfluidic paper-based systems, and potentiometric probes (Bandodkar et al., 2019; Booth et al., 2021; Ibupoto et al., 2012; Li et al., 2023; Nguyen et al., 2022; Schyrr et al., 2014; Shitanda et al., 2023; Zheng et al., 2024). Although these methods offer interesting routes toward non-invasive monitoring, many suffer from inadequate sensitivity, slow response times, or limited stability in complex biofluids. Electrochemical sensing (lactate and pH) remains one of the most promising because of its scalability, low power requirements, inherent sensitivity, and compatibility with miniaturized, point-of-care platforms (Adib et al., 2025a; Saha et al., 2022; Seymour et al., 2021; Uchayash et al., 2025). However, critical limitations persist in the translation of existing electrochemical platforms to complex biological matrices. Recently reported amperometric lactate biosensors including Nafion-membrane-based LOx platforms and flexible wearable patches, have advanced sensitivity and miniaturization, but operate under fixed, pre-calibrated pH conditions and rely on passive permselective membranes to manage interfering species (García-Guzmán et al., 2024; Xuan et al., 2021; Yang and Yan, 2025). Crucially, none of these platforms incorporates active, feedback-controlled regulation of the local electrochemical microenvironment, leaving LOx catalytic efficiency vulnerable to the dynamic pH fluctuations intrinsic to saliva, a limitation explicitly acknowledged even in the most advanced wearable platforms, where passive polymeric outer layers represent the current state-of-the-art for pH compensation (Rind et al., 2025). Furthermore, antifouling strategies in reported lactate biosensors have predominantly relied on perfluorinated membranes such as Nafion (Reza et al., 2024), which raise significant environmental and regulatory concerns as per- and polyfluoroalkyl substances (PFAS) (Lohmann et al., 2020). Most reported platforms also address lactate or pH detection independently, without co-integrated sensing and active pH control on a single chip, limiting their utility in dynamic biological settings.

In this work, we present a fully integrated multiplexed interdigitated microelectrode (IDE)-based biosensor capable of simultaneous lactate and pH detection with in-situ electrochemical pH control (Fig. 1). Building on our previous IDE platform for glucose sensing with localized pH modulation (Adib et al., 2025a), this study extends the approach to lactate detection, which presents distinct kinetic behavior and oxygen dependence compared to glucose oxidase-based systems. The differing optimal pH window and stability characteristics of LOx required re-optimization of the protonator parameters and enzymatic interface. Given that salivary lactate is a stress- and hypoxia-associated biomarker in calves, this work advances the platform toward analyte-specific optimization and real-sample validation for livestock monitoring. Unlike commercial lactate meters designed for invasive blood testing and single-point analysis, the proposed system is tailored for operation in complex biofluids such as saliva and for repeated on-animal measurements. Gold IDEs were fabricated using multilayer photolithography and modified with platinum black (Pt-B), o-phenylenediamine (o-PD), β-cyclodextrin (β-CD), and LOx to form a selective lactate sensing interface. Finite element simulations guided optimization of proton transport and localized pH gradients, while electrochemical and structural characterization (SEM, EDX, AFM, CV, CA, EIS) confirmed stable platform performance. The use of β-CD as a PFAS-free permselective layer exploiting host-guest molecular recognition for selective exclusion of small electroactive interferents represents a conceptual departure from the conventional fluorinated polymer membranes such as Nafion employed in recently reported electrochemical lactate sensors (Reza et al., 2024; Xuan et al., 2021), while in-situ electrochemical pH control is adapted here to actively regulate the local sensing microenvironment in a salivary lactate biosensing context, rather than passively tolerating pH variability as in existing platforms (Rind et al., 2025; Yang and Yan, 2025). Together, these two features constitute the principal conceptual advancement of the present work over the current state of the art. β-CD enhanced anti-interference capability through selective host-guest interactions (Zhu et al., 2020). To enable field deployment, a portable, battery-powered electronics interface supporting CV, CA, and pH control with wireless data transmission was developed. The portable system produced results comparable to benchtop instrumentation and was validated using saliva from healthy and clinically unwell calves. The platform successfully differentiated animals based on lactate and pH signatures, demonstrating its potential as a non-invasive tool for longitudinal, on-farm health monitoring. Together, this work establishes a multiplexed, pH-regulated sensing platform for practical livestock

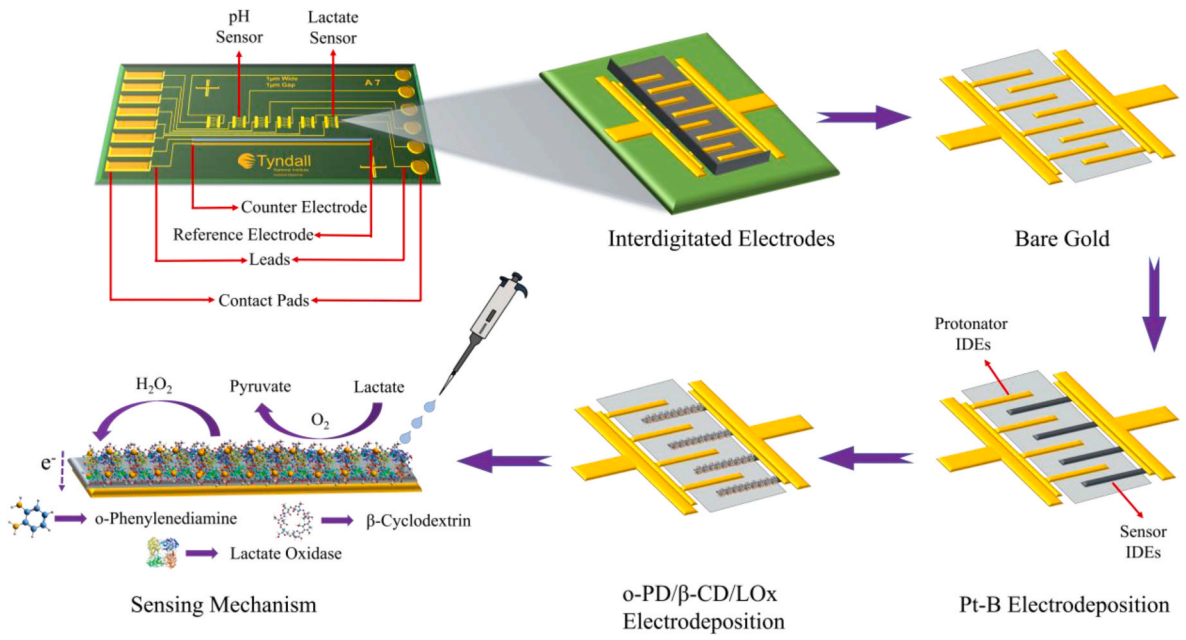


Fig. 1. (a) Schematic representation of the integrated IDE-based multiplexed platform illustrating electrode allocation within the chip, including the counter electrode (CE), reference electrode (RE), six working electrodes (WEs), and designated functional roles: lactate-sensing WE, pH-sensing WE, and protonator IDEs for localized electrochemical pH control, along with contact pads and leads. (b) Image of individual sensing electrode. (c) Schematic of the surface modification process for lactate oxidase immobilization on to the interdigitated microband array electrodes. (d) Sensing mechanism of lactate detection at the electrode solution interface.

diagnostics.

2. Materials and methods

2.1. Materials and reagents

Experimental details, including materials, instrumentation, and electrochemical setup, are provided in the **Supplementary data.**

2.2. Sensor fabrication

The fabrication of IDE array chips was carried out using standard microfabrication techniques, including photolithography, metal deposition, lift-off, and etching. The overall process was adapted from previously reported methods (Adib et al., 2020, 2025b; Dawson et al., 2013; Juska et al., 2023; Schuller et al., 2019). Detailed fabrication procedures, numerical simulation methodology for local pH modulation, and additional characterization protocols are provided in the **Supplementary data.**

2.3. Electrochemical measurements

All electrochemical measurements were performed using a custom-designed chip holder equipped with a sample well sealed to the chip via a fluoroelastomer O-ring. A top lid, secured with screws, ensured stable and leak-free contact during measurements. In this study, lactate detection was achieved indirectly by quantifying the H_2O_2 generated as a by-product of the enzymatic reactions of lactate. To confirm the electrode's ability to detect H_2O_2, the modified electrode surface (Pt-B/o-PD/β-CD) was first tested with varying concentrations of H_2O_2 in the absence of LOx. Electrochemical experiments, including CV and CA, were then conducted to evaluate both pH sensing and lactate detection. The bare Au electrodes were used to monitor pH variations from pH 3 to 9, while the Pt-B/o-PD/β-CD/LOx-modified electrodes were employed to measure known concentrations of lactate within physiologically relevant ranges in 10 mM PB (pH 7.4). Electrochemical pH control was further examined through sequential CV and CA experiments for both the pH and lactate biosensing platforms. The LOD for each analyte was calculated as three times the standard deviation (σ) of the blank (PB solution) divided by the slope (S) of the calibration curve:

$$LOD = 3.3 \times \frac{\sigma}{S} \quad (1)$$

For calibration plots displayed on a semi-logarithmic axis, the LOD was determined using an equivalent form of the same expression. In the low-concentration region, the local sensitivity was approximated from the measured response at a known concentration using $S \approx I/C$, where C is the known lactate concentration in the low-concentration region and I is the corresponding measured current magnitude at that concentration. Substitution into the classical expression yields (Kong et al., 2021)**:**

$$LOD = \frac{3.3 \times \sigma \times C}{I} \quad (2)$$

To assess selectivity, the biosensor response was tested in the presence of potential interfering species typically found in saliva, including 0.5 mM of AA, UA, D-Fruc, D-Glu, and Ace. These tests were carried out with 2 mM and 5 mM lactate in 10 mM PB (pH 7.4) using CA measurements. Stability tests were performed by recording the response to 2 mM lactate over a period of 40 days under refrigerated storage conditions. Additional experiments were carried out using artificial saliva to evaluate both pH and lactate detection with active pH control, employing CV and CA techniques via both the Autolab potentiostat and a custom-built electronic interface. Finally, the biosensor was validated using eight real calf saliva samples with known disease statuses to verify its diagnostic capability. Due to sample volume limitations, two representative samples (one healthy and one diseased) were selected for detailed analysis of lactate detection and pH modulation using both measurement systems. The local pH was optimized to 6.0 during real-sample testing to achieve accurate quantification of lactate concentration. For comparison, a commercial lactate meter was also employed to measure lactate levels in the same saliva samples. It should be noted that the commercial meter was used in the present study as a comparative reference platform to provide preliminary benchmarking rather than as an absolute gold-standard saliva assay. Data analysis, including linear regression and slope determination for calibration plots, was conducted

using OriginPro 2021 software. All calibration data were obtained from three independent measurements (n = 3), and error bars represent the standard deviation of the mean.

2.4. Lactate measurement with in-situ pH control

Initial CA measurements were performed with varying concentrations of lactate prepared in PB (pH 7.4), as LOx exhibits its highest catalytic activity near this pH (Xu et al., 1996). However, because the pH of saliva fluctuates with health status, precise pH regulation was required to enhance measurement reproducibility, maintain enzyme performance, and promote the generation of molecular oxygen during sensing. Although the optimal enzymatic activity of LOx typically occurs around pH 7.4, electrochemical pH control was employed to locally adjust the pH value to pH 6.0 for standardization across saliva pH variability and to facilitate the electrochemical production of molecular oxygen, which was estimated using Faraday's first law of electrolysis:

$$n = \frac{Q}{F \times v} \tag{3}$$

where n represents the number of moles of substance liberated, Q is the total charge passed, F is Faraday's constant, and v is the ionic valency. Using this relationship, it was estimated that approximately 3×10^9 molecules/s of O_2 were generated near the sensing electrodes upon applying a positive potential to the protonator IDEs. Detailed calculations are provided in the Supplementary data. The presence of sufficient oxygen ensured continuous regeneration of the oxidized form of LOx, thereby preventing oxygen diffusion limitations typically encountered in first-generation oxidase-based amperometric sensors (Weigelt et al., 1987). For measurements in artificial saliva (pH 6.8), in-situ electrochemical pH control was achieved by applying a constant anodic potential to the protonator IDEs, generating both protons (H^+) and molecular oxygen (O_2) according to Eq. (4), thereby reducing the local pH near the sensing IDEs. A potential of 1.05 V (versus on-chip reference electrode) was applied to shift the pH from 6.8 to 6.0. This approach relies on the water splitting process and the reaction mechanism is as follows (Abdullah et al., 2021):

$$Anode: 2H_2O \rightarrow O_2 + 4H^+ + 4e^- \tag{4}$$

$$Cathode: 2H^+ + 2e^- \rightarrow H_2 \tag{5}$$

2.5. IoT-enabled custom sensor interface for electrochemical analysis

A custom-designed portable PCB potentiostat was developed for real-time lactate and pH monitoring in calf saliva. The system was adapted from a previously reported electrochemical disease detection platform (Murphy, 2023) and built around the ADuCM355 System-on-Chip (Analog Devices), which integrates a Cortex-M3 microcontroller with an analog front end optimized for electrochemical sensing (Adib et al., 2021). The interface enables multiplexed electrochemical measurements and wireless data transmission to a smartphone. Detailed hardware architecture, firmware implementation, power management, and communication protocols are provided in the **Supplementary data.**

2.6. Calf health assessment

Calf health was monitored twice weekly on two non-consecutive days from birth until weaning, using a structured clinical scoring approach described previously (Sinnott et al., 2024). Each calf was evaluated across eleven health parameters: demeanor, mobility, interest in surroundings, rectal temperature, ear position, eye condition, nasal discharge, fecal consistency, presence of cough, navel appearance, and joint condition, based on the framework adapted for dairy calves (Barry et al., 2022). Each health indicator was assigned a score on a 0-3 scale, where 0 represented a normal, healthy condition and 3 denoted a severe abnormality. Following every assessment, results were promptly communicated to the farm manager to facilitate timely treatment decisions. Calves exhibiting signs of illness received appropriate care, either by farm staff or under veterinary supervision, depending on the severity and complexity of the case. Details regarding treatment type and duration were systematically recorded for each health episode. When a calf's health score indicated the need for veterinary attention, a saliva sample was collected from that individual. Simultaneously, a paired saliva sample was obtained from a healthy calf within the same age group to serve as a control. Saliva collection followed the procedure outlined in the literature (Rubio et al., 2021), employing a sterile foam oral swab (Sterile Oral Swab Mouthcare, Medguard Healthcare). Each calf was allowed to chew the swab for approximately 1 min to ensure sufficient sample volume. The collected swabs were then processed to extract saliva, which was immediately prepared for biochemical and electrochemical analysis.

2.7. Statistical analysis

Statistical analyses were performed using OriginPro 2021. Agreement between the proposed biosensor platform and the commercial Lactate Pro 2 analyzer was evaluated using least-squares linear regression analysis. The slope and intercept were determined from the covariance of the two datasets, and goodness-of-fit was assessed using the coefficient of determination (R^2), calculated from the Pearson correlation coefficient. The mean absolute error (MAE) between the two methods was also calculated to quantify analytical agreement. Intra-group variability was assessed using mean ± standard deviation (SD) and coefficient of variation (CV%). All calibration measurements were performed in triplicate (n = 3), and error bars represent ±1 standard deviation unless otherwise stated. Analytical accuracy was assessed by comparing biosensor-measured lactate concentrations against values obtained from a commercial lactate meter (Lactate Pro 2) across eight calf saliva samples. A paired Student's t-test was performed with significance set at α = 0.05 (two-tailed), with the 95% confidence interval (CI) reported. The t-statistic (t), degrees of freedom (df), and probability value (p) are reported alongside CI values where applicable. Recovery (%) was calculated as (measured/reference) × 100. Intraday and interday precision were evaluated over the validated operational lifetime of the sensor (Days 1-35), as progressive sensitivity loss was observed beyond this point. Intraday precision was expressed as the relative standard deviation (RSD%) of triplicate measurements (n = 3) performed on each test day, calculated as $RSD\% = (\sigma_i / \mu_i) \times 100\%$. Interday precision was determined from the standard deviation of daily mean responses across 8 test days, expressed as $RSD\% = (\sigma_{inter} / \overline{\mu}) \times 100\%$. where σ_i is the standard deviation of triplicate measurements on day i, μ_i is the corresponding mean current response, $\overline{\mu}$ is the grand mean of all daily mean current responses, and n is the number of test days. Due to the limited cohort size for real saliva validation (n = 8, diseased n = 2), diagnostic performance metrics are presented as preliminary.

3. Results and discussion

3.1. Electrochemical characterization

The electrochemical performance of the IDE platform was validated using cyclic voltammetry in 1 mM ferrocenecarboxylic acid (FCA), exhibiting diffusion-limited behavior characteristic of microelectrode arrays due to overlapping radial diffusion zones (Seymour et al., 2026) (Fig. S4a). Excellent inter- and intra-chip reproducibility was observed (RSD = 0.3%), confirming stable electrode fabrication and reliable on-chip reference and counter electrodes. Generator-collector measurements displayed quasi steady-state profiles consistent with ultramicroelectrode array behavior (Wahl et al., 2018), with a collection efficiency of ~82% (Fig. S4b). This high efficiency supports effective proton transport between protonator and sensing IDEs, enabling

localized pH modulation. Optimization studies identified 10 mM o-phenylenediamine (o-PD) and 10 mg/mL LOx as optimal modification conditions (Fig. S4c and d), with maximal LOx activity observed near pH 7.5 (Fig. S4e), consistent with previously reported kinetic profiles for this enzyme. These optimized conditions were carried forward for all subsequent lactate detection experiments. Additional structural and electrochemical characterization data, including SEM, EDX, AFM, CV, EIS, and step-by-step surface modification verification, are provided in the **Supplementary data.**

3.2. pH-dependent gold oxide reduction behavior

A detailed simulation study exploring gold oxide as a pH sensor is presented in the **Supplementary data** section. The formation and reduction of gold oxide have been extensively studied and can be represented by the following reaction (Burke and Nugent, 1997; Kennedy et al., 2026):

$$2Au + 3H_2O \rightleftarrows Au_2O_3 + 6H^+ + 6e^- \quad (6)$$

In this work, an oxide layer was generated on the gold IDEs by CV, sweeping the potential to approximately 1.0 V (vs. on-chip Pt) to induce oxide formation, followed by a reverse cathodic sweep to reduce the gold oxide back to metallic gold. The reduction peak minima obtained during this reverse scan were used as a pH-dependent signal, since the potential of the gold oxide reduction shifts linearly with the hydrogen ion concentration of the surrounding medium. To evaluate the pH response, CVs were recorded across a series of buffer solutions (pH 3-9), scanning between −0.2 V and 1.0 V. Each measurement was repeated three times to confirm reproducibility. The overlaid CVs in Fig. 2a show a systematic anodic shift in the gold oxide reduction potential with decreasing pH. The observed decrease in current intensity of the gold oxide reduction peaks at lower pH values resulted from maintaining a constant potential window since the oxide formation peaks also move anodically, less oxide is formed within the available voltage range. The reduction potential minima values, corresponding to each pH, were plotted versus pH to establish the calibration curve using the on-chip Pt RE (Fig. 2b). The data exhibited excellent linearity ($R^2 = 0.999$) with a super-Nernstian slope of −66.0 mV.pH^{-1} (n = 3). This enhanced response may arise from the formation of multilayer gold oxides, a phenomenon also reported for other metal oxide-based pH sensors such as iridium and ruthenium oxides (Manjakkal et al., 2020). The minimal standard deviations across replicates further confirmed the reliability of this pH sensing approach. To experimentally validate the simulation model for electrochemical pH control, additional CV measurements were performed in PB while applying a steady potential to the protonator IDEs. Unlike the galvanostatic method used in simulations, a potentiostatic approach was chosen here to ensure precise control over the applied potential and local proton generation. Fig. 2c compares CV scans before and after activating electrochemical pH control. The black curve corresponds to a chemically adjusted pH 6.8 (saliva pH), while the red curve represents the same solution where the pH was electrochemically reduced to 6.0 by applying 1.05 V at the protonator IDEs. Upon activation, the gold oxide reduction peak shifted anodically to approximately 0.24 V, matching the reduction potential recorded for buffer pH 6.0 in Fig. 2a. This correspondence confirms that the in-situ electrochemical pH control effectively modulated the local environment to the desired pH level, validating the accuracy of the simulation results.

3.3. Electrochemical detection of lactate

Since the lactate detection in this system relies on the enzymatic production of H_2O_2, the sensor's direct electrochemical response to H_2O_2 was characterized first. Fig. 3a shows the CVs recorded at the Au/Pt-B/o-

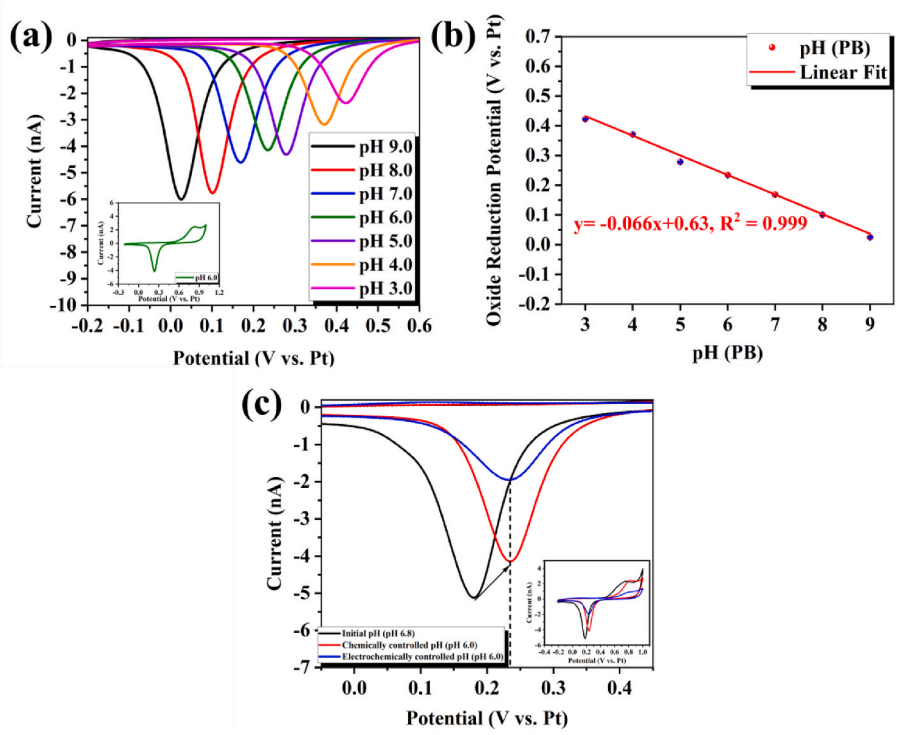


Fig. 2. (a) Zoomed in portion of CVs showing gold oxide reduction peaks obtained at gold microband electrodes in pH buffer solution ranging from pH 3 to 9 with Pt reference electrode at a scan rate of 100 mV/s. The inset shows the full CV scan used to take a measurement. (b) Corresponding calibration plot of reduction potential verses different pH. (c) Electrochemically obtained CVs from pH buffer at an initial pH 6.8 (since the pH of the artificial saliva is pH 6.8) by using on-chip Pt reference electrode, the oxide reduction peak is seen at approximately 0.18 V (black). pH was controlled by biasing the protonator electrodes array at 1.05 V, the oxide reduction peak shifts to 0.234 V (blue) which is the same match as the buffer pH 6.0 (red). Error bars represent standard deviation (n = 3). (For interpretation of the references to color in this figure legend, the reader is referred to the Web version of this article.)

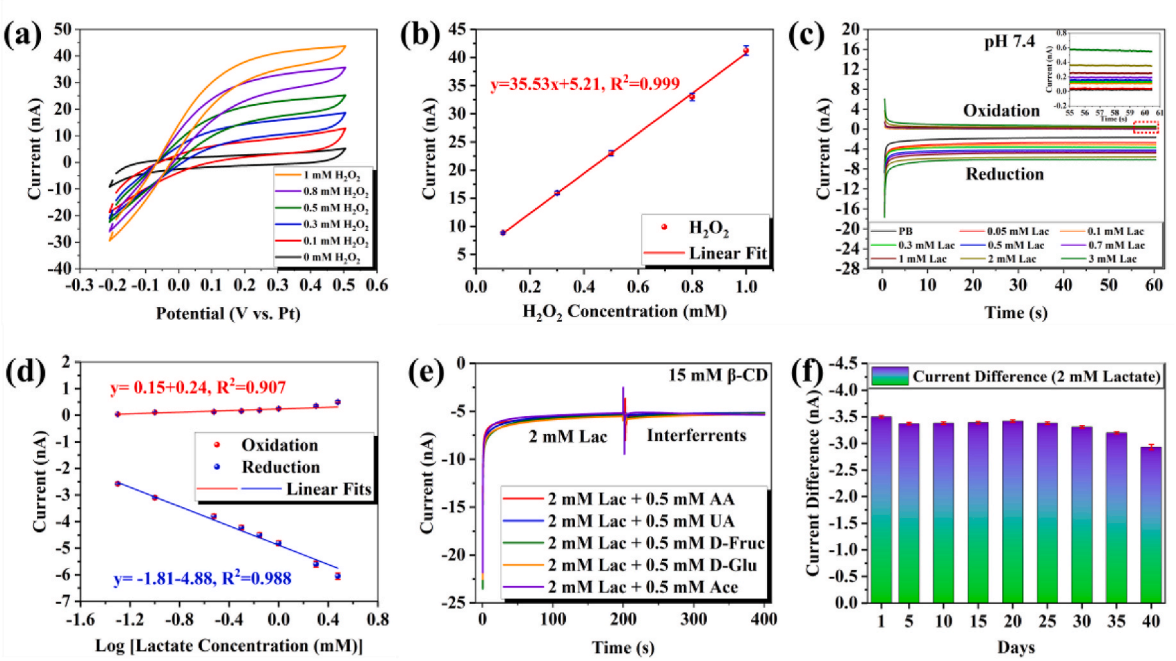


Fig. 3. (a) Cyclic voltammograms (CVs) of the Au/Pt-B/o-PD/β-CD surface for oxidation to increase H_2O_2 concentrations with on-chip reference electrode. (b) Corresponding calibration plots obtained at 0.25 V for the oxidative responses of H_2O_2. (c) Chronoamperometric (CA) responses of the Au/Pt-B/o-PD/β-CD/LOx surface for oxidation and reduction of increasing lactate concentrations in 10 mM PB. Inset shows the last 5 s responses for oxidation. (d) The resulting calibration plots and linear range of the biosensor in semi-log scale. (e) CA responses of 2 mM lactate (10 mM PB, pH 7.4) and aliquots of 2 mM lactate + other potential interfering species (L-ascorbic acid (AA), uric acid (UA), D-fructose (D-Fruc), D-Glucose (D-Glu), and Acetaminophen (Ace)) added after 200 s of the measurement. All the error bars represents the standard deviation obtained from the last 5 s of averaged three cycles (n = 3) time of measurement. (f) Long-term stability of the lactate biosensor in 2 mM lactate concentration for 40 days. Data beyond Day 35 reflect progressive sensitivity loss attributed to enzyme degradation or surface matrix changes. Error bars represent standard deviation (n = 3).

PD/β-CD modified IDEs in the presence of increasing concentrations of H_2O_2 using the on-chip Pt reference electrode. Measurements were performed over the potential window of −0.2 to 0.5 V (vs. on-chip Pt) at a scan rate of.

50 mV s^{-1}. The CVs displayed a clear and systematic rise in anodic current with increasing H_2O_2 concentration, illustrating the catalytic oxidation of H_2O_2 at the Pt-B modified electrodes. The oxidation current increased progressively from 0 mM (black curve) to 1.0 mM H_2O_2 (orange curve), confirming excellent electrochemical sensitivity toward H_2O_2. The most pronounced enhancement in current was observed around 0.2-0.3 V, where the Pt-black nanostructured layer provides a high-surface-area interface that accelerates electron transfer. The well-separated and concentration-dependent anodic waves demonstrate that the o-PD/β-CD film remains permeable to H_2O_2, enabling efficient diffusion of the analyte to the underlying Pt-B catalytic sites. This confirmed that the polymeric layer does not hinder H_2O_2 transport, an essential prerequisite for reliable lactate detection, as the amperometric signal in this system depends entirely on efficient diffusion of LOx-generated H_2O_2 to the underlying Pt-B catalytic sites. To quantify this response, the anodic current was plotted as a function of H_2O_2 concentration, and the corresponding calibration curve is shown in Fig. 3b. Error bars represent standard deviation (n = 3), derived from three consecutive CVs at each concentration. The calibration exhibited excellent linearity with an R^2 value of 0.999 and a sensitivity of 35.53 nA mM^{-1}. The LOD was calculated to be 2.98 μM, confirming that sensors display a highly linear and predictable response to H_2O_2 across the tested concentration range. The CA responses of lactate measurement obtained at ±0.25 V for 60 s in 10 mM PB (pH 7.4) are shown in Fig. 3c. In both the oxidative and reductive modes, the faradaic current increased proportionally with lactate concentration over the range of 0.05-3 mM, which lies within the physiologically relevant salivary lactate levels for calves (Contreras-Aguilar et al., 2021). In all cases, the biosensor reached a steady-state current within 20 s, demonstrating rapid response characteristics. The corresponding calibration plots for oxidation and reduction are presented in Fig. 3d, both of which show strong linearity with R^2 values of 0.907 (oxidation) and 0.988 (reduction). The full lactate concentration profile was displayed using a semi-logarithmic axis to accommodate the wide dynamic range (Kong et al., 2021). The calculated sensitivities from the slope of the calibration curves were 0.15 nA mM^{-1} for the oxidative signal and −1.81 nA mM^{-1} for the reductive signal in PB. The theoretical LOD were determined to be 7.7 μM (oxidation) and 4.1 μM (reduction). The reductive response of LOx-generated H_2O_2 clearly outperforms the oxidative mode, exhibiting greater sensitivity and a lower LOD. Consequently, all subsequent lactate measurements in this study were conducted using the electrochemical reduction method.

3.4. *Selectivity and long-term stability of the lactate biosensor*

Interfering species are a major challenge in salivary lactate sensing, prompting a detailed evaluation of the biosensor's resistance to common electroactive compounds. The analytes such as AA, UA, D-Fruc, D-Glu, and Ace are routinely reported in saliva and can compromise lactate measurements if not adequately suppressed (Dongiovanni et al., 2023; Ngamchuea et al., 2018; Zhang et al., 2025). Conventional lactate sensors frequently incorporate PFAS based membranes such as Nafion to enhance selectivity. However, PFAS coatings pose several disadvantages, including their strong dependence on humidity and temperature can adversely affect reproducibility, the polymer can hinder lactate transport to the electrode surface, and their environmental persistence and bioaccumulation present significant ecological and health concerns (Pandelides et al., 2025). To address these limitations, β-CD was implemented as the selective layer. Owing to its hydrophilic exterior and hydrophobic internal cavity, β-CD can host small organic molecules such

as lactate, while effectively limiting interference from electroactive contaminants. Its solubility and stability in aqueous media make it particularly well-suited for saliva-based sensing applications (Kwon et al., 2015; Xia et al., 2024).

Selectivity measurements were performed in 10 mM phosphate buffer containing 2 mM lactate (with 10 mg mL^{-1} LOx), to which interferents were added at concentrations exceeding their physiological levels. The chronoamperometric responses in Fig. 3e were recorded at −0.25 V for 400 s. During the first 200 s, only lactate was present, interferents were introduced at 200 s, and the remaining 200 s captured the biosensor's response. Small current transients observed at the injection point were attributed to briefly opening the Faraday cage during interferrent addition. Importantly, the recorded currents showed minimal deviation in the presence of any of the interfering species, demonstrating strong selectivity. The relative current changes ($I_0/I \times 100$), where Io is the interfering substance, I is the measured lactate current, are summarized in Table S3 in the **Supplementary data** along with further analysis. Long-term stability was assessed by storing the modified sensors at 4 °C in 10 mM PB for 40 days. As shown in Fig. 3f, a gradual reduction in current response toward 2 mM lactate was observed over time, likely due to enzyme degradation or changes in the polymer/enzyme matrix. Despite this decline, the sensor maintained an RSD of 2.57% across Days 1-35, indicating good long-term stability within its validated lifetime. These findings confirm that the Au/Pt-B/o-PD/β-CD/LOx biosensor exhibits excellent selectivity and robust performance as well as possible applicability of lactate detection in calf saliva. To extend shelf life further, additional storage strategies such as low-humidity environments, inert atmospheres, addition of stabilizing agents such as dextrose, refrigeration, or vacuum conditions may be beneficial.

3.5. Lactate and pH monitoring in artificial and calf saliva

Since buffer-based measurements do not fully capture the complexity of biological fluids, the performance of the lactate and pH sensors was next examined in artificial saliva to assess their behavior in a more realistic medium. Fig. 4a shows the calibration plots obtained from CA, highlighting the effect of pH adjustment on analytical performance with detail explanation provided in the **Supplementary data**. A control electrode fabricated without LOx yielded a flat baseline (black trace), verifying that the analytical current originated exclusively from the enzymatic reaction. Under pH-controlled conditions in artificial saliva, the sensor achieved a sensitivity of −0.51 nA mM^{-1} and a theoretical LOD of 0.6 μM, representing performances comparable to measurements conducted without pH control, while offering improved operational stability under saliva-relevant conditions. The primary benefit of pH control is to improve the operational stability/robustness under saliva-relevant conditions. Despite this enhancement, the overall signal amplitude in saliva remained lower than that observed in PB. This reduction is expected given the complex physicochemical environment of saliva, which contains proteins, growth factors, electrolytes, and exhibits higher viscosity than simple buffer systems (Bi et al., 2023; Canon et al., 2018; Forszt et al., 2025). Higher viscosity reduces diffusivity and mass transport, which can decrease the diffusion-limited current (Chang et al., 2023; Demchenko et al., 1989). In addition to lactate detection, pH measurements were performed using CV in artificial saliva **(Supplementary data)**. The resulting calibration curve produced a linear relationship ($R^2 = 0.956$) between the oxide reduction potential and pH, with a sensitivity of −119 mV.pH^{-1}, confirming reliable pH sensing capability even within the more challenging saliva matrix, which is shown in Fig. 4b. Notably, the unspiked artificial-saliva trace acquired

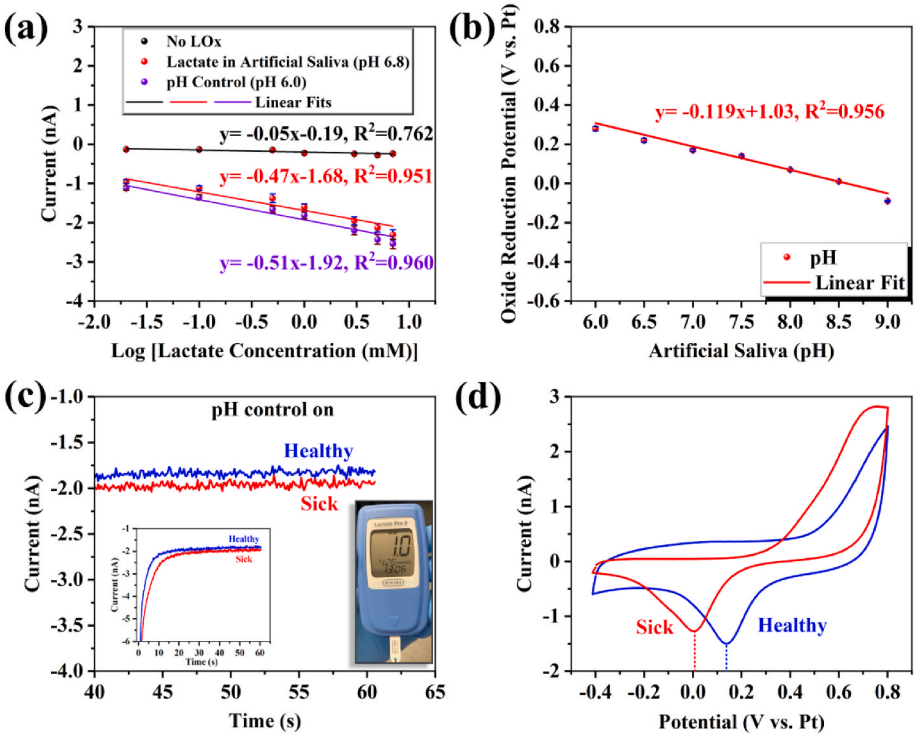


Fig. 4. (a) Semi-logarithmic calibration plots derived from chronoamperometric (CA) responses of a No-LOx control electrode, an LOx-modified electrode in artificial saliva at pH 6.8, and an LOx-modified electrode under pH-controlled conditions (pH 6.0), achieved by biasing the protonator array electrodes at 1.05 V. Linear regression fits and corresponding R^2 values are shown. (b) Resulting calibration plot attained from the Cyclic voltammograms of bare gold electrodes in artificial saliva pH solutions ranging from pH 6.0 to 9.0 with on chip reference electrode at a scan rate of 100 mV/s (c) CA responses during the last 20 s obtained from the biosensor in calf saliva samples for lactate detection under pH-controlled conditions. Inset shows the full CA traces and corresponding measurements from a commercial lactate meter. (d) CVs of calf saliva samples for pH determination. Error bars represent standard deviation (n = 3). (For interpretation of the references to color in this figure legend, the reader is referred to the Web version of this article.)

under active protonation (Fig. S7b), recorded with the sensing electrode held at −0.25 V while the protonator was biased at +1.05 V, constitutes a lactate-free background under continuous oxygen generation, its preservation relative to the protonator-off condition (Fig. S7a) indicates that deliberate oxygen generation does not introduce significant cathodic interference at the sensing potential. Consistent with this, the CA traces obtained in undiluted calf saliva under continuous protonation (Figs. 4c and 5e) reached stable steady states without current discontinuities attributable to gas-bubble occlusion.

Saliva samples from eight calves (from Teagasc research farm) were analyzed to evaluate pH and lactate levels. Initial lactate measurements were acquired without applying in-situ pH control, and the corresponding chronoamperometric data for all animals are shown in Fig. S8. To quantitatively evaluate agreement between the proposed platform and the commercial Lactate Pro 2 analyzer across all eight samples (healthy and sick) (Table S4), least-squares linear regression analysis was performed **(Supplementary data).** The regression yielded $Y = 0.937X + 48.23$ with $R^2 = 0.987$, indicating strong correlation between the two methods. The MAE was 16.5 μM, corresponding to an average relative error of 2.32%. Moreover, salivary lactate concentrations measured by the biosensor demonstrated clear separation between healthy (586-713 μM, n = 6) and diseased calves (966-1005 μM, n = 2), consistent with measurements obtained using the commercial lactate meter (Table S4). The elevated salivary lactate concentrations observed in the two diseased calves (966-1005 μM) suggest metabolic stress and were used to classify these animals as clinically abnormal. A paired Student's t-test further confirmed no statistically significant difference between the two methods across all eight samples (t = 0.24, df = 7, p = 0.82, 95% CI = [−18.88, 15.38] μM), with a mean recovery of 100.5% and recovery %RSD of 2.8% (range: 96.6-104.8%), demonstrating excellent analytical accuracy. A mean recovery of 100.5% is considered acceptable as it indicates close agreement between measured and reference values, consistent with established biosensor analytical validation criteria (Sergeev et al., 2007). The recovery %RSD of 2.8% compares favorably with values reported in the literature for analogous LOx-based electrochemical lactate biosensors operating in biological matrices, including RSD values of 2.7-5.1% (Madden et al., 2022), up to 8.4% (Sainz et al., 2022), ≤6.6% (Pohanka and Zboril, 2008), ≤10% (Ghimenti et al., 2020), and 2.5-13.0% across multiple biosensor platforms (Rathee et al., 2016) confirming the superior precision of the developed biosensor. The precision of the lactate biosensor was further evaluated over its validated 35-day operational lifetime. Intraday RSD% values ranged from 0.64% to 1.00% (mean 0.79%), confirming excellent within-day repeatability of the sensor response. The interday RSD%, computed across 8 test days spanning the full 35-day period, was 2.57%, demonstrating consistent and reproducible performance throughout the operational window. Similarly, while the paired Student's t-test (p = 0.82) and mean recovery of 100.5% demonstrate excellent analytical performance, these results are derived from a limited sample set of eight animals. Full analytical validation will therefore require testing across larger, disease-balanced cohorts spanning multiple farms, seasons, and disease severity levels.

Given that pH control enables regulation of the local sensing environment, testing under pH-regulated conditions was also undertaken. However, limited sample volume allowed complete analysis only for two representative calves, one previously identified as healthy (calf 6) and one as unwell (calf 8). Lactate detection under pH-controlled operation for both animals is shown in Fig. 4c, with the corresponding commercial lactate meter results provided in the inset. The pH measurements obtained by CV are shown in Fig. 4d, and quantitative values are included in Table S5. Under pH-controlled conditions, both the lactate and pH values for calf 6 was within the expected physiological range for healthy animals (Contreras-Aguilar et al., 2021; Reid and Huffman, 1949). In contrast, calf 8 displayed substantially altered pH and lactate levels, consistent with disease-associated metabolic perturbation. These electrochemical results correlate strongly with the independent calf health scoring, which classified calf 6 as healthy and calf 8 as clinically unwell (Table S6). For context, a comparison of the analytical performance of the developed biosensor with previously reported enzymatic lactate sensors is provided in Table S7, highlighting the competitive sensitivity and applicability of the present platform for salivary diagnostics.

3.6. *Performance of portable sensor interface for salivary lactate and pH detection*

To enable on-site, real-time monitoring of salivary lactate and pH, a

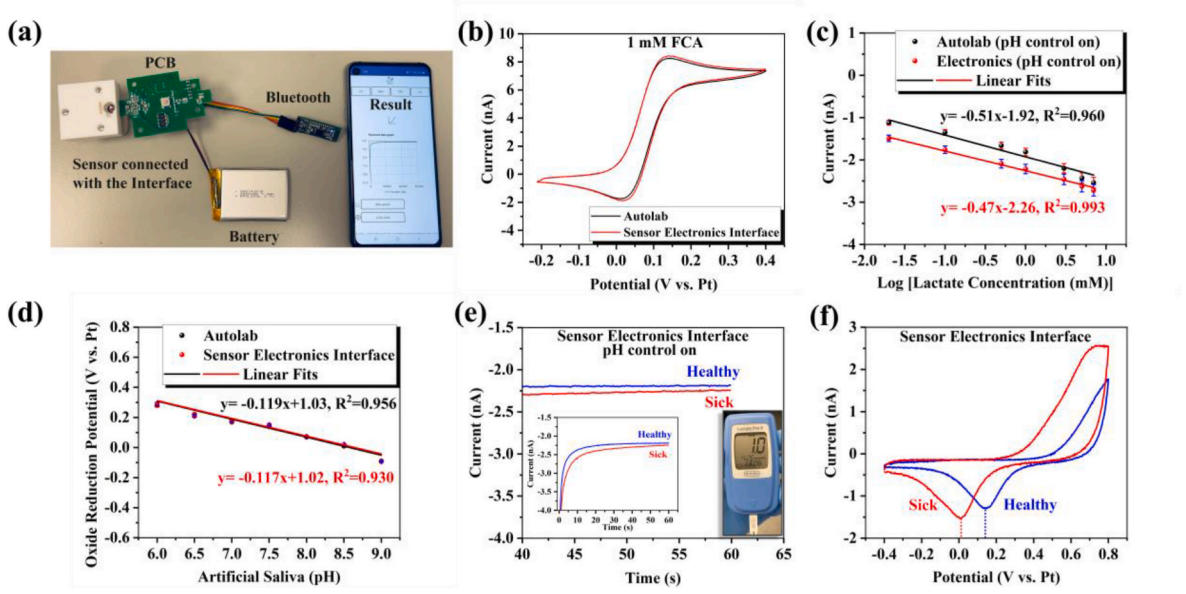


Fig. 5. (a) A comprehensive view of the developed biosensor along with its interface electronics. (b) CVs of both Autolab and Sensor electronics interface in 1 mM FCA. Response comparison plots acquired from CA for the (c) Lactate and (d) pH sensors measured by Autolab potentiostat and sensor electronics interface. (e) CA responses during the last 20 s obtained from the biosensor in calf saliva samples for lactate detection under pH-controlled conditions using sensor electronics interface. Inset shows the full CA traces and corresponding measurements from a commercial lactate meter. (f) CVs calf saliva samples for pH determination using sensor electronics interface. Error bars represent standard deviation (n = 3).

custom-designed portable sensor interface was developed and integrated with the IDE-based sensing platform. Lactate and pH signals were acquired from independent working electrodes on the same IDE chip using a simultaneous approach (CA for lactate and CV for pH), demonstrating integrated multiplex capability within a single sample droplet. In all CA measurements, the lactate signal was quantified from the final 20 s of the 60 s acquisition window, by which point the response had reached steady state and any capacitive transient associated with establishing the protonator bias had fully decayed, rendering the reported signal insensitive to switching-induced charging effects. The complete system consists of the microfabricated sensor chip connected to a compact battery-powered PCB, incorporating an analog front-end, a multiplexer for electrode selection, and a Bluetooth Low Energy module for wireless data transfer to a smartphone. An overview of the assembled system is shown in Fig. 5a, while the simplified readout circuit and functional block diagrams are provided in Fig. S9. Before evaluating salivary analytes, the performance of the portable interface was benchmarked against a laboratory instrument using 1 mM FCA as an electrochemical probe. As shown in Fig. 5b, the cyclic voltammograms obtained from both platforms exhibited excellent overlap, demonstrating that the portable interface accurately replicates the electrochemical response achieved using the laboratory setup. This confirmed the reliability of the custom hardware for both voltammetric and amperometric measurements. Following this benchmarking, lactate and pH sensing experiments were performed using the portable interface under the same analytical conditions used for the laboratory system. Lactate detection in artificial saliva was carried out both with and without in-situ pH control along with the pH measurements, and the results were compared directly with those from the laboratory instrument **(Supplementary data)**. Fig. 5c presents the comparison using CA-based calibration for lactate sensing with pH control enabled. The portable interface achieved a sensitivity of −0.47 nA mM^{-1}, closely matching the value obtained using the laboratory instrument. A small current offset (approximately −0.113 nA) was observed in the portable device, which is consistent with baseline shifts typically encountered in compact, battery-driven electrochemical circuits. Importantly, this offset did not influence analytical performance, as it remained constant across measurements. The pH measurements recorded using the portable interface also aligned strongly with laboratory results. As shown in Fig. 5d, the CVs of the gold oxide reduction peaks yielded a sensitivity of −117 $mV.pH^{-1}$, in excellent agreement with the laboratory measurements. Only minimal differences were observed between the two platforms, demonstrating that the miniaturized system maintains high precision and reproducibility for both pH and lactate sensing.

To confirm real-sample applicability, the portable interface was further evaluated using saliva from calf 6 (healthy) and calf 8 (unwell). Fig. 5e and f presents the lactate and pH measurements obtained from both animals. The data from the portable interface closely match the results obtained using the laboratory setup, validating the consistency of the portable system. The comparative performance metrics are summarized in Table 1. While analytical metrics are comparable to commercial meters, our platform is designed for integration and operation in saliva-like matrices with localized electrochemical control, enabling future continuous or on-animal monitoring. Consistent with the laboratory measurements and calf health scoring, calf 6 exhibited lactate and pH values within the expected physiological range, while calf 8 showed significantly altered values indicative of disease. Together, these results establish that the portable sensor interface performed equivalently to the laboratory system, offering accurate, stable, and reproducible detection of lactate and pH in saliva. The successful operation of the compact electronics, combined with wireless data transfer and low-power operation, demonstrates its strong potential for on-farm diagnostics, field monitoring, and future integration into wearable health-monitoring systems for livestock.

4. Conclusions and future perspective

This study presents the successful development of a highly sensitive, non-invasive salivary pH and lactate sensor system based on IDE arrays. The platform integrates an in-situ electrochemical pH control strategy with a custom-designed portable sensor interface, enabling precise local pH regulation and enhanced analyte detection. The pH control mechanism generates molecular oxygen, which improves LOx activity and enables fine adjustment of the local pH near the sensing electrode, even under mildly acidic conditions. Finite element simulations and electrochemical experiments using gold IDEs confirmed the feasibility of this localized microenvironment control strategy. The close spacing between protonator and sensing electrodes enabled reliable pH adjustment to approximately pH 6.0, ensuring optimal lactate measurements in saliva. Structural and electrochemical characterization using SEM, EDX, AFM, and EIS verified successful electrode modification and enzyme immobilization through electropolymerized o-PD/β-CD/LOx films, supporting efficient electron transfer and catalytic stability. The pH sensor demonstrated a linear response from pH 3-9 (R^2 = 0.999) with a sensitivity of −66.0 $mV.pH^{-1}$ in buffer, and −119 $mV.pH^{-1}$ (Autolab) and −117 $mV.pH^{-1}$ (portable electronics) in artificial saliva. The lactate sensor exhibited linear ranges of 0.05-3 mM (R^2 = 0.988) in buffer and 0.02-7 mM in artificial saliva, achieving a limit of detection of 0.6 μM (artificial saliva) and sensitivities of −0.51 nA mM^{-1} (Autolab) and −0.47 nA mM^{-1} (portable electronics). Incorporation of β-CD improved selectivity by suppressing interference from AA, UA, D-fruc, D-glu, and Ace. The sensors showed rapid response times (<20 s) and stable performance for up to one month, with moderate sensitivity loss beyond 35 days due to enzyme or surface degradation. Both sensors successfully quantified pH and lactate in calf saliva, effectively distinguishing healthy from diseased animals using both laboratory instrumentation and the portable electronics interface. Despite these promising results, biological validation was conducted on a limited sample cohort and under controlled testing conditions. Long-term operational stability in continuous on-farm environments remains to be fully established. Future work will therefore prioritize prospective validation across larger and disease-balanced animal cohorts, a prerequisite for establishing clinically meaningful diagnostic thresholds alongside enhancing enzyme stabilization and antifouling surface strategies to extend sensor lifetime, validating performance across larger animal populations, and integrating the IDE platform into automated or wearable saliva sampling systems. Further miniaturization and system-level optimization may enable continuous, real-time livestock health monitoring, advancing the translation of this multiplexed sensing approach toward field-deployable precision animal diagnostics.

Table 1
Performance comparison of conventional testing setup and sensor electronics interface for pH and lactate sensing.

Samples	Calf ID	Autolab Potentiostat	Sensor Electronics Interface	Autolab Potentiostat	Sensor Electronics Interface	Commercial Lactate Meter Measurement (μM)	Calf Health Visualization
		pH		Lactate Concentration (μM)	Lactate Concentration (μM)		
				pH Control on	pH Control on		
Calf-6	**2049**	**7.51**	**7.52**	**703 ± 12**	**686 ± 36**	**700 ± 100**	**Healthy**
Calf-8	**2202**	**8.52**	**8.57**	**1036 ± 15**	**1029 ± 27**	**1000 ± 120**	**Sick**

CRediT authorship contribution statement

Md Ridwan Adib: Conceptualization, Data curation, Investigation, Methodology, Visualization, Writing – original draft. **Javier Higes-Marquez:** Software. **Colm Barrett:** Formal analysis, Methodology, Visualization. **Shane O'Sullivan:** Software. **Marie McFadden:** Resources. **Emer Kennedy:** Conceptualization, Supervision, Writing – review & editing. **Alan O'Riordan:** Conceptualization, Funding acquisition, Supervision, Writing – review & editing.

Declaration of competing interest

The authors declare that they have no known competing financial interests or personal relationships that could have appeared to influence the work reported in this paper.

Acknowledgments

This research was supported by the VistaMilk Research Centre, Research Ireland (RI), and the Department of Agriculture, Food and the Marine on behalf of the Government of Ireland under Grant Number [21/RC/10303_P2]. Ethical approval for calf sample collection was obtained from the Teagasc Animal Ethics Committee [TAEC2022-351], and a license was granted by the Health Products Regulatory Authority [AE19132/P165]. The authors thank Brendan Sheehan for his assistance with AFM sample processing and for his valuable input during data analysis discussions. The authors also acknowledge Marcello Valente for his support with testing the sensor electronics interface. The support of Zoetis Inc. is also gratefully acknowledged.

Appendix A. Supplementary data

Supplementary data to this article can be found online at https://doi.org/10.1016/j.bios.2026.118965.

Data availability

Data will be made available on request.

References

Abdullah, U., Ali, M., Pervaiz, E., 2021. Mol. Catal. 508, 111575. https://doi.org/10.1016/j.mcat.2021.111575.
Adib, M.R., Barrett, C., O'Sullivan, S., Flynn, A., McFadden, M., Kennedy, E., O'Riordan, A., 2025a. Biosens. Bioelectron. 275, 117234. https://doi.org/10.1016/j.bios.2025.117234.
Adib, M.R., Kennedy, E., O'Riordan, A., 2025b. Presented at the 2025 IEEE SENSORS. IEEE, Vancouver, BC, Canada, pp. 1–4. https://doi.org/10.1109/SENSORS59705.2025.11330345.
Adib, M.R., Kondalkar, V.V., Lee, K., 2020. Adv. Mater. Technol. 5, 2000009. https://doi.org/10.1002/admt.202000009.
Adib, M.R., Lee, Y., Kondalkar, V.V., Kim, S., Lee, K., 2021. ACS Sens. 6, 1012–1021. https://doi.org/10.1021/acssensors.0c02219.
All-Island Animal Disease Surveillance Report, 2022. URL. https://www.animalhealthsurveillance.agriculture.gov.ie/currentnews/all,island,disease,surveillance,report,2022.html.
Arakawa, T., Kuroki, Y., Nitta, H., Chouhan, P., Toma, K., Sawada, S., Takeuchi, S., Sekita, T., Akiyoshi, K., Minakuchi, S., Mitsubayashi, K., 2016. Biosens. Bioelectron. 84, 106–111. https://doi.org/10.1016/j.bios.2015.12.014.
Attree, E., Griffiths, B., Panchal, K., Xia, D., Werling, D., Banos, G., Oikonomou, G., Psifidi, A., 2024. Commun. Biol. 7, 1251. https://doi.org/10.1038/s42003-024-06925-9.
Bandodkar, A.J., Gutruf, P., Choi, J., Lee, K., Sekine, Y., Reeder, J.T., Jeang, W.J., Aranyosi, A.J., Lee, S.P., Model, J.B., Ghaffari, R., Su, C.-J., Leshock, J.P., Ray, T., Verrillo, A., Thomas, K., Krishnamurthi, V., Han, S., Kim, J., Krishnan, S., Hang, T., Rogers, J.A., 2019. Sci. Adv. 5. https://doi.org/10.1126/sciadv.aav3294 eaav3294.
Barrett, C., Dawson, K., O'Mahony, C., O'Riordan, A., 2015. ECS J. Solid State Sci. Technol. 4, S3053–S3058. https://doi.org/10.1149/2.0141510jss.
Barry, J., Bokkers, E.A.M., Sayers, R., Murphy, J.P., De Boer, I.J.M., Kennedy, E., 2022. J. Dairy Sci. 105, 560–571. https://doi.org/10.3168/jds.2021-20343.
Berman, J., 2024. Animals 14, 329. https://doi.org/10.3390/ani14020329.
Bi, Y., Sun, M., Wang, J., Zhu, Z., Bai, J., Emran, M.Y., Kotb, A., Bo, X., Zhou, M., 2023. Anal. Chem. 95, 6690–6699. https://doi.org/10.1021/acs.analchem.3c00361.
Blakebrough-Hall, C., McMeniman, J.P., González, L.A., 2020. J. Anim. Sci. 98. https://doi.org/10.1093/jas/skaa005 skaa005.
Bonilla-Cedrez, C., Steward, P., Rosenstock, T.S., Thornton, P., Arango, J., Kropff, M., Ramirez-Villegas, J., 2023. Nat. Sustain. 6, 1279–1286. https://doi.org/10.1038/s41893-023-01161-1.
Booth, M.A., Gowers, S.A.N., Hersey, M., Samper, I.C., Park, S., Anikeeva, P., Hashemi, P., Stevens, M.M., Boutelle, M.G., 2021. Anal. Chem. 93, 6646–6655. https://doi.org/10.1021/acs.analchem.0c05108.
Burke, L.D., Nugent, P.F., 1997. Gold Bull. 30, 43–53. https://doi.org/10.1007/BF03214756.
Canon, F., Neiers, F., Guichard, E., 2018. J. Agric. Food Chem. 66, 7873–7879. https://doi.org/10.1021/acs.jafc.8b01998.
Castillo-Lopez, E., Petri, R.M., Ricci, S., Rivera-Chacon, R., Sener-Aydemir, A., Sharma, S., Reisinger, N., Zebeli, Q., 2021. J. Dairy Sci. 104, 4875–4892. https://doi.org/10.3168/jds.2020-19142.
Chang, C., Lee, C.-Y., Tai, N.-H., 2023. ACS Appl. Nano Mater. 6, 3936–3947. https://doi.org/10.1021/acsanm.3c00119.
Contreras-Aguilar, M.D., Monkeviciene, I., Ceron, J.J., Silinskas, I., Vallejo-Mateo, P.J., Tecles, F., Martinez-Subiela, S., Tvarijonaviciute, A., Zelvyte, R., 2019. Res. Vet. Sci. 124, 383–386. https://doi.org/10.1016/j.rvsc.2019.04.019.
Contreras-Aguilar, M.D., Vallejo-Mateo, P.J., Lamy, E., Escribano, D., Cerón, J.J., Tecles, F., Rubio, C.P., 2021. Animals 11, 749. https://doi.org/10.3390/ani11030749.
d'Amone, L., Matzeu, G., Omenetto, F.G., 2021. ACS Biomater. Sci. Eng. 7, 5451–5473. https://doi.org/10.1021/acsbiomaterials.1c01138.
Dawson, K., Baudequin, M., Sassiat, N., Quinn, A.J., O'Riordan, A., 2013. Electrochim. Acta 101, 169–176. https://doi.org/10.1016/j.electacta.2012.09.105.
Demchenko, A.P., Rusyn, O.I., Saburova, E.A., 1989. Biochim. Biophys. Acta Protein Struct. Mol. Enzymol. 998, 196–203. https://doi.org/10.1016/0167-4838(89)90273-2.
Department of Agriculture, 2022. Food, and the Marine Report. URL. https://www.gov.ie/en/department-of-agriculture-food-and-the-marine/collections/dafm-annual-reports/.
Dokur, E., Gorduk, O., Sahin, Y., 2025. FlatChem 51, 100848. https://doi.org/10.1016/j.flatc.2025.100848.
Dongiovanni, P., Meroni, M., Casati, S., Goldoni, R., Thomaz, D.V., Kehr, N.S., Galimberti, D., Del Fabbro, M., Tartaglia, G.M., 2023. Int. J. Oral Sci. 15, 27. https://doi.org/10.1038/s41368-023-00231-6.
Doyle, D., Credille, B., Lehenbauer, T.W., Berghaus, R., Aly, S.S., Champagne, J., Blanchard, P., Crossley, B., Berghaus, L., Cochran, S., Woolums, A., 2017. Veterinary Internal Medicine, vol. 31, pp. 954–959. https://doi.org/10.1111/jvim.14683.
Forszt, D., Gerreth, K., Karpienko, K., Zalewska, A., Hojan, K., Marchewka, R., Bielas, M., Maciejczyk, M., 2025. Sci. Rep. 15, 12676. https://doi.org/10.1038/s41598-025-97974-5.
García-Guzmán, J.J., Jiménez Heras, J.M., López-Iglesias, D., González-Álvarez, R.J., Cubillana-Aguilera, L., González Macías, C., Fernández Alba, J.J., Palacios-Santander, J.M., 2024. Microchim. Acta 191, 526. https://doi.org/10.1007/s00604-024-06602-y.
Ghimenti, S., Lomonaco, T., Bellagambi, F.G., Biagini, D., Salvo, P., Trivella, M.G., Scali, M.C., Barletta, V., Marzilli, M., Di Francesco, F., Errachid, A., Fuoco, R., 2020. Sci. Rep. 10, 7441. https://doi.org/10.1038/s41598-020-64112-2.
Ibupoto, Z.H., Shah, S.M.U.A., Khun, K., Willander, M., 2012. Sensors 12, 2456–2466. https://doi.org/10.3390/s120302456.
Ike, K., Muto, K., Hioki, T., Loew, N., Shitanda, I., Takesue, M., Okuda, M., 2025. ACS Sens. 10, 4707–4716. https://doi.org/10.1021/acssensors.5c01238.
Joseph, P.A., Doluweera, D., Chandraratne, A., Balasubramaniam, B., Abeyratne, V., Hewa, S.P., Rambukwella, R., Wanigasuriya, K.P., Indrakumar, J., Perera, N., 2025. BMC Infect. Dis. 25, 438. https://doi.org/10.1186/s12879-025-10810-z.
Juska, V.B., Maxwell, G.D., O'Riordan, A., 2023. Biosens. Bioelectron. X 13, 100315. https://doi.org/10.1016/j.biosx.2023.100315.
Kappes, A., Tozooneyi, T., Shakil, G., Railey, A.F., McIntyre, K.M., Mayberry, D.E., Rushton, J., Pendell, D.L., Marsh, T.L., 2023. Front. Vet. Sci. 10, 1168649. https://doi.org/10.3389/fvets.2023.1168649.
Kennedy, K., Adib, M.R., Rönnby, K., Seymour, I., Nolan, M., O'Riordan, A., 2026. Electrochim. Acta 567, 148791. https://doi.org/10.1016/j.electacta.2026.148791.
Kong, D., Zhao, J., Tang, S., Shen, W., Lee, H.K., 2021. Anal. Chem. 93, 12156–12161. https://doi.org/10.1021/acs.analchem.1c02011.
Kwon, T., Jeong, Y.K., Deniz, E., AlQaradawi, S.Y., Choi, J.W., Coskun, A., 2015. ACS Nano 9, 11317–11324. https://doi.org/10.1021/acsnano.5b05030.
Li, J., Zhu, Y., Shoemake, B., Liu, B., Adkins, P., Wallace, L., 2022. J. Vet. Diagn. Invest. 34, 577–586. https://doi.org/10.1177/10406387221081232.
Li, Y., Luo, S., Gui, Y., Wang, X., Tian, Z., Yu, H., 2023. Biosensors 13, 287. https://doi.org/10.3390/bios13020287.
Lohmann, R., Cousins, I.T., DeWitt, J.C., Glüge, J., Goldenman, G., Herzke, D., Lindstrom, A.B., Miller, M.F., Ng, C.A., Patton, S., Scheringer, M., Trier, X., Wang, Z., 2020. Environ. Sci. Technol. 54, 12820–12828. https://doi.org/10.1021/acs.est.0c03244.
Lorenz, I., Fagan, J., More, S.J., 2011. Ir. Vet. J. 64, 9. https://doi.org/10.1186/2046-0481-64-9.
Madden, J., Vaughan, E., Thompson, M., O' Riordan, A., Galvin, P., Iacopino, D., Rodrigues Teixeira, S., 2022. Talanta 246, 123492. https://doi.org/10.1016/j.talanta.2022.123492.
Malon, R.S.P., Chua, K.Y., Wicaksono, D.H.B., Córcoles, E.P., 2014. Analyst 139, 3009–3016. https://doi.org/10.1039/C4AN00201F.
Manjakkal, L., Szwagierczak, D., Dahiya, R., 2020. Prog. Mater. Sci. 109, 100635. https://doi.org/10.1016/j.pmatsci.2019.100635.

Mentzoni, F., Skaugen, M., Eythorsdottir, I., Roterud, S., Johansen, E.S., Losnegard, T., 2024. Eur. J. Appl. Physiol. 124, 3781–3788. https://doi.org/10.1007/s00421-024-05572-6.
Murphy, A., 2023. Electrochemical Sensor Interface (Thesis). University College Cork. Ireland.
Ngamchuea, K., Chaisiwamongkhol, K., Batchelor-McAuley, C., Compton, R.G., 2018. Analyst 143, 81–99. https://doi.org/10.1039/C7AN01571B.
Nguyen, D., Lawrence, M.M., Berg, H., Lyons, M.A., Shreim, S., Keating, M.T., Weidling, J., Botvinick, E.L., 2022. ACS Sens. 7, 441–452. https://doi.org/10.1021/acssensors.1c01720.
Omole, O.O., Nappert, G., Naylor, J.M., Zello, G.A., 2001. J. Nutr. 131, 2128–2131. https://doi.org/10.1093/jn/131.8.2128.
Otten, N.D., Skarbye, A.P., Krogh, M.A., Michelsen, A.M., Nielsen, L.R., 2023. Acta Vet Scand, vol. 65, p. 45. https://doi.org/10.1186/s13028-023-00708-8.
Pandelides, Z., Arblaster, J., Pandelides, A.F., Nichols, E., Thapalia, A., Conder, J., 2025. Integrated Environmental Assessment and Management vjaf142. https://doi.org/10.1093/inteam/vjaf142.
Pardon, B., Buczinski, S., 2020. Veterinary Clinics of North America: Food Animal Practice, vol. 36, pp. 425–444. https://doi.org/10.1016/j.cvfa.2020.03.005.
Pietraforte, D., Castelli, M., Metere, A., Scorza, G., Samoggia, P., Menditto, A., Minetti, M., 2006. Free Radic. Biol. Med. 41, 1753–1763. https://doi.org/10.1016/j.freeradbiomed.2006.08.014.
Pohanka, M., Zboril, P., 2008. Food Technol. Biotechnol. 46, 107–110. https://hrcak.srce.hr/22234.
Rathee, K., Dhull, V., Dhull, R., Singh, S., 2016. Biochem. Biophys. Rep. 5, 35–54. https://doi.org/10.1016/j.bbrep.2015.11.010.
Reid, J.T., Huffman, C.F., 1949. J. Dairy Sci. 32, 123–132. https://doi.org/10.3168/jds.S0022-0302(49)92019-6.
Reza, M.S., Seonu, S., Abu Zahed, M., Asaduzzaman, M., Song, H., Hoon Jeong, S., Park, J.Y., 2024. Talanta 270, 125582. https://doi.org/10.1016/j.talanta.2023.125582.
Riley, B.B., Corbishley, A., Haskell, M.J., Duthie, C.-A., Macrae, A.I., Burrough, E., Mason, C., 2024. Front. Vet. Sci. 11, 1483890. https://doi.org/10.3389/fvets.2024.1483890.
Rind, S., Zhang, N., Khan, W.U., Zhang, Q., 2025. Wearable Electronics, vol. 2, pp. 323–343. https://doi.org/10.1016/j.wees.2025.08.002.
Roblin, M., Canniere, E., Barbier, A., Daandels, Y., Dellevoet-Groenewegen, M., Pinto, P., Tsaousis, A., Leruste, H., Brainard, J., Hunter, P.R., Follet, J., 2023. Current research in parasitology & vector-borne. Diseases 4, 100149. https://doi.org/10.1016/j.crpvbd.2023.100149.
Rubio, C.P., Escribano, D., Mainau, E., Cerón, J.J., Navarro, E., Manteca, X., 2021. BMC Vet. Res. 17, 373. https://doi.org/10.1186/s12917-021-03087-2.
Saha, T., Songkakul, T., Knisely, C.T., Yokus, M.A., Daniele, M.A., Dickey, M.D., Bozkurt, A., Velev, O.D., 2022. ACS Sens. 7, 2037–2048. https://doi.org/10.1021/acssensors.2c00830.
Sainz, R., Pozo, M.D., Vázquez, L., Vilas-Varela, M., Castro-Esteban, J., Blanco, E., Petit-Domínguez, M.D., Quintana, C., Casero, E., 2022. Anal. Chim. Acta 1208, 339851. https://doi.org/10.1016/j.aca.2022.339851.
Sapurta, H.A., Karim, M.M., 2025. Electrochemical science. Advances 5, 1–26. https://doi.org/10.1002/elsa.202400021.
Schuller, P., Rothbauer, M., Eilenberger, C., Kratz, S.R.A., Höll, G., Taus, P., Schinnerl, M., Genser, J., Ertl, P., Wanzenboeck, H., 2019. MethodsX 6, 2606–2613. https://doi.org/10.1016/j.mex.2019.10.038.
Schyrr, B., Pasche, S., Scolan, E., Ischer, R., Ferrario, D., Porchet, J.-A., Voirin, G., 2014. Sensor. Actuator. B Chem. 194, 238–248. https://doi.org/10.1016/j.snb.2013.12.032.
Sergeev, N.V., Herold, K.E., Rasooly, A., 2007. In: Marks, R.S., Cullen, D.C., Karube, I., Lowe, C.R., Weetall, H.H. (Eds.), Handbook of Biosensors and Biochips. Wiley. https://doi.org/10.1002/9780470061565.hbb132.
Seymour, I., Barry, F., O'Riordan, A., Rohan, J.F., 2026. Sensor. Actuator. B Chem. 446, 138689. https://doi.org/10.1016/j.snb.2025.138689.
Seymour, I., O'Sullivan, B., Lovera, P., Rohan, J.F., O'Riordan, A., 2021. ACS Sens. 6, 1030–1038. https://doi.org/10.1021/acssensors.0c02264.
Shehta, A., El-Zahar, H., Mansour, A., Mustafa, B., Shety, T., 2022. Beni-Suef Univ J Basic Appl Sci 11, 128. https://doi.org/10.1186/s43088-022-00309-w.
Shitanda, I., Ozone, Y., Morishita, Y., Matsui, H., Loew, N., Motosuke, M., Mukaimoto, T., Kobayashi, M., Mitsuhara, T., Sugita, Y., Matsuo, K., Yanagita, S., Suzuki, T., Mikawa, T., Watanabe, H., Itagaki, M., 2023. ACS Sens. 8, 2368–2374. https://doi.org/10.1021/acssensors.3c00490.
Singh, S., Sharma, P., Pal, N., Sarma, D.K., Tiwari, R., Kumar, M., 2024. ACS Infect. Dis. 10, 808–826. https://doi.org/10.1021/acsinfecdis.3c00625.
Sinnott, A.M., Bokkers, E.A.M., Murphy, J.P., McPherson, S., Sugrue, K., Kennedy, E., 2024. Livest. Sci. 284, 105492. https://doi.org/10.1016/j.livsci.2024.105492.
Song, M., Bai, H., Zhang, P., Zhou, X., Ying, B., 2023. Int. J. Oral Sci. 15, 2. https://doi.org/10.1038/s41368-022-00209-w.
Stoytcheva, M., Velkova, Z., Gochev, V., Valdez, B., Curiel, M., 2025. Int. J. Electrochem. Sci. 20, 100924. https://doi.org/10.1016/j.ijoes.2024.100924.
Uchayash, S., Que, S.S., Rubby, M.F., Kabir, M.I., Que, L., 2025. ACS Appl. Nano Mater. 8, 11404–11414. https://doi.org/10.1021/acsanm.5c01308.
Wahl, A.J.C., Seymour, I.P., Moore, M., Lovera, P., O'Riordan, A., Rohan, J.F., 2018. Electrochim. Acta 277, 235–243. https://doi.org/10.1016/j.electacta.2018.04.181.
Weigelt, D., Schubert, F., Scheller, F., 1987. Analyst 112, 1155. https://doi.org/10.1039/an9871201155.
Xia, D.-X., Xu, C.-Y., Ye, M.-F., Lin, R.-L., Liu, J.-X., 2024. ACS Appl. Mater. Interfaces 16, 45745–45753. https://doi.org/10.1021/acsami.4c09782.
Xu, P., Yano, T., Yamamoto, K., Suzuki, H., Kumagai, H., 1996. Appl. Biochem. Biotechnol. 56, 277–288. https://doi.org/10.1007/BF02786958.
Xuan, X., Pérez-Ràfols, C., Chen, C., Cuartero, M., Crespo, G.A., 2021. ACS Sens. 6, 2763–2771. https://doi.org/10.1021/acssensors.1c01009.
Yang, H., Yan, S., 2025. Int. J. Electrochem. Sci. 20, 101132. https://doi.org/10.1016/j.ijoes.2025.101132.
Zhang, Z., Wang, S., Chen, T., Wang, H., Dou, Q., 2025. Nanoscale 17, 13698–13707. https://doi.org/10.1039/D5NR01340B.
Zheng, X.T., Goh, W.P., Yu, Y., Sutarlie, L., Chen, D.Y., Tan, S.C.L., Jiang, C., Zhao, M., Ba, T., Li, H., Su, X., Yang, L., 2024. Adv. Healthcare Mater. 13. https://doi.org/10.1002/adhm.202302173.
Zhou, Y., Liu, Z., 2023. Clin. Chim. Acta 548, 117503. https://doi.org/10.1016/j.cca.2023.117503.
Zhu, L., Liu, X., Yang, J., He, Y., Li, Y., 2020. Anal. Chem. 92, 11981–11986. https://doi.org/10.1021/acs.analchem.0c02430.